ACS Sustainable Chemistry & Engineering

pubs.acs.org/journal/ascecg

Research Article

Advancing Waste Plastic Valorization: Catalytic Production of Aviation Fuel over Zeolite and Ru/CNT-Based Catalysts

Karoline Kaiser Ferreira,[†] Mariana Rita Tuna Oliveira Costa,[†] Lucília S. Ribeiro,* José J. M. Órfão, and Manuel Fernando R. Pereira

Cite This: *ACS Sustainable Chem. Eng.* 2026, 14, 4042−4052

Read Online

ACCESS | Metrics & More | Article Recommendations | Supporting Information

ABSTRACT: This work investigates the hydroprocessing of polyolefins using both model and waste plastics. A catalyst screening using low-density polyethylene (LDPE) identified Ru/CNT_{ox} + HY (Si/Al = 24) and Ru/CNT_{ox} + CNT_{ox} + HY as the most effective systems for producing hydrocarbons in the aviation fuel range (C_8−C_{16}). Under optimized conditions (i.e., 325 °C, 30 bar H_2, 3 h), the Ru/CNT_{ox} + HY catalytic system produced up to 80% liquids in the C_8−C_{16} range with significant isomerization (iso/*n* = 4). When applied to real plastic residues, such as used pipet tips and a plastic bag, C_8−C_{16} selectivities of 80−90% in the liquid phase were achieved, with iso/*n* ratios of up to 9. These results highlight the potential of combining carbon-supported metal catalysts with zeolites as a robust bifunctional catalytic system for the valorization of plastic waste into high-quality aviation fuel, contributing to sustainable solutions for plastic management and energy production.

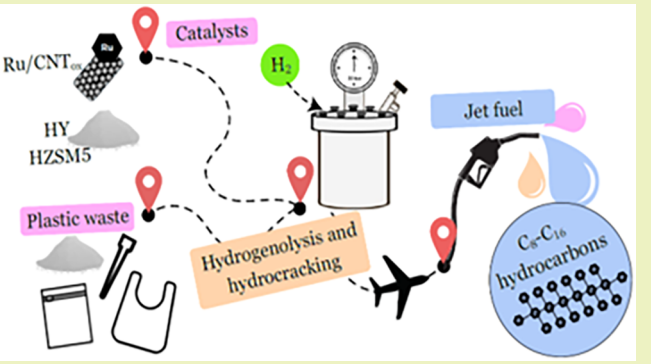

KEYWORDS: *Ru/CNT_{ox} catalysts, zeolites, hydrocracking, plastic upcycling, jet fuel*

1. INTRODUCTION

The accumulation of plastic waste and the growth of the aviation sector pose critical environmental challenges with potentially harmful consequences and, therefore, require innovative solutions. Aviation remains heavily dependent on fossil-derived fuels, and its decarbonization is hindered by strict fuel specifications and technological challenges associated with alternative energy adoption.[1] Simultaneously, if the current plastic consumption and waste management practices remain the same, it is expected that 12 billion tons of plastic will end up in landfills, worsening their global oversaturation.[2,3]

Since traditional mechanical recycling methods are insufficient to address this issue, chemical recycling has been regarded as a promising pathway to enhance plastic recyclability.[4,5] Additionally, sustainable aviation fuels (SAF) are agreed to be one of the most promising options to decrease greenhouse gas emissions in the short and medium term. SAF is composed of hydrocarbons within the same carbon number range as conventional jet fuel, typically from C_8 to C_{16}, but derived from renewable or waste-based feedstocks, enabling fuel compatibility.[1]

Catalytic cracking has received particular attention, as several studies have demonstrated its ability to convert plastics into various fuel types, providing an effective upgrading pathway even under mild temperature and pressure conditions.[4−10] Hydroconversion of plastic polymers under hydrogen atmospheres emerges as a promising approach since this process can produce a variety of products, including hydrocarbon fuels within the jet fuel range (C_8−C_{16}), thereby representing a potential synergetic solution to both issues. A life-cycle assessment study by Azam et al.[11] revealed that hydrocracking exhibits better environmental performance in 10 out of 11 impact categories compared to pyrolysis, another thermochemical process capable of yielding gaseous and liquid fuels.

Hydrocracking relies on metal-catalyzed C−H activation and acid-catalyzed C−C bond cleavage, typically employing metals on acidic supports, whereas hydrogenolysis is usually carried out at lower temperatures with both C−H activation and C−C cleavage occurring at metal sites.[6] The most commonly used catalysts for hydrocracking are bifunctional systems that combine metal sites for hydrogenation with Brønsted acid sites on the support to promote isomerization and cracking, making them ideal for these reactions and desired out-

Received: November 6, 2025
Revised: February 10, 2026
Accepted: February 11, 2026
Published: February 19, 2026

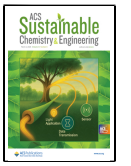

https://doi.org/10.1021/acssuschemeng.5c12040
ACS Sustainable Chem. Eng. 2026, 14, 4042−4052

comes.[8,12,13] On the other hand, for hydrogenolysis, the most common are metal supported on metal-oxides.[6,8]

Regarding the catalyst support, carbon nanotubes (CNTs) present themselves as an interesting option for hydrocracking. Carbon materials are widely used as catalyst supports due to their stability under various reaction conditions. CNTs, in particular, are attractive supports because of their physico-chemical properties—namely the high surface area, high thermal and mechanical stability, good electrical conductivity, hydrophobic nature, and strong metal—support interactions, combined with the possibility to control their porosity and absence of micropores.[14,15]

Studies with various metal phases and supports can be found in the literature. For instance, Jia et al.[7] studied various carbon-supported metal catalysts, namely Ru, Cu, Fe, Ni, Pt, Pd, and Rh, and the Ru catalyst relayed the most favorable results, with a liquid product yield of over 90% when using *n*-hexane as a solvent for 1 h of reaction at 220 °C and 60 bar of H_2. Chen et al.[16] also studied some of these carbon-supported catalysts (Ru, Pd, Rh, and Ni), as well as Ir, without the use of any solvent, and also concluded that the Ru catalyst yielded the best results, with a liquid product yield of over 57% at 175 °C and 82 bar of H_2. In fact, Ru as an active phase promotes the cleavage of C−C bonds, a pivotal step in breaking larger polymeric chains into smaller hydrocarbons.[7,8] It is also worth noting that other studies have proven success in plastic catalytic cracking without the use of solvents, which offers process, logistical, and environmental advantages.[9,10,13,17,18]

Additionally, zeolites have been shown to catalyze polymer cracking, even in the absence of a metal phase. Costa et al.[13] reported full conversion of low-density polyethylene (LDPE) using HZSM5 as a monofunctional catalyst. Various other studies have also used zeolites as supports for metal phases with satisfactory results.[9,18,19]

Recent advances have explored the combination of metal catalysts supported on metal oxides with acidic zeolites to enhance the polymer hydrocracking. Several studies[20−24] have reported that noble metals supported on oxide-based materials, when combined with zeolites, exhibit strong synergistic effects between metallic and Brønsted acid sites, improving the overall catalytic performance. However, despite the recognized benefits of carbon materials as catalyst supports, the use of Ru supported on CNT combined with zeolites remains largely unexplored.

This study aims to synthesize, characterize, and evaluate bifunctional Ru-based catalysts supported on oxidized CNT (CNT_{ox}) and also physically mixed with zeolites (HY and HZSM5) for solvent-free catalytic hydroconversion of LDPE. The main objective is to maximize the production of jet fuel range hydrocarbons, an end-goal that is not particularly common in the realms of hydroconversion from this type of feedstock.[25] Within the scope of this article, the term hydrocarbons from the jet fuel range is used to refer to the C_8−C_{16} fraction derived from plastic waste. To the best of the authors' knowledge, no hydrocracking study of plastic has been conducted using this catalytic system. Thus, this study aims to explore the suitability of this novel catalytic system for the jet fuel range hydrocarbon production application.

2. EXPERIMENTAL METHODS

2.1. Chemicals

Nanocyl-7000 multiwalled CNTs (90%) were provided by Nanocyl. Ammonium-type zeolite Y (SiO_2:Al_2O_3 mole ratio 12:1) and ZSM5 (SiO_2/Al_2O_3 mole ratio 30:1) were purchased from Alfa Aesar. The precursor $RuCl_3{\cdot}xH_2O$ (99%) was purchased from Sigma-Aldrich, while HNO_3 and *n*-hexane (95%) were acquired from VWR. Powdered LDPE was purchased from Goodfellow and employed as a model plastic. In addition, a used LDPE market plastic bag, LDPE ziplock sample bags, and discarded polypropylene (PP) pipet tips were selected as representative waste plastics.

2.2. Synthesis of Materials

First, the zeolites were calcined under an air flow (100 $cm^3\ min^{-1}$) at 600 °C for 3 h to obtain their acid forms (HY and HZSM5). To introduce oxygen-containing surface groups, which contribute to increasing the surface acidity and enhancing metal dispersion, CNTs were treated with HNO_3 (7 mol L^{-1}) and heated to the boiling point for 3 h. Afterward, the material was washed with distilled water until reaching neutral pH and then dried at 110 °C for 24 h, hereafter referred to as CNT_i. This sample was further treated under a N_2 flow (100 $cm^3\ min^{-1}$) at 250 °C for 3 h; the resulting material was denoted CNT_{ox}. This thermal treatment was carried out to evaluate the influence of heat treatment on the support properties, since oxygen-containing surface groups begin to decompose at temperatures around 200 °C, which can affect the total acidity of the catalyst.[26] In this case, after impregnation, the catalyst was submitted to a thermal treatment under N_2, followed by a reduction under H_2, both at 250 °C.

A monometallic catalyst containing 2.5 wt % Ru was synthesized by incipient wetness impregnation, employing an aqueous solution of the respective metal precursor, which was added dropwise onto CNT_i. The impregnated material was then dried overnight at 110 °C in an oven, followed by thermal treatment in a tubular furnace under a N_2 flow (100 $cm^3\ min^{-1}$) at 250 °C for 3 h. Subsequently, a reduction step was carried out under a H_2 flow (100 $cm^3\ min^{-1}$) at 250 °C for 3 h. The resulting catalyst was named Ru/CNT_{ox}. All flow rates are expressed under standard conditions.

2.3. Characterization Techniques

The textural properties of the catalysts were determined by N_2 adsorption at −196 °C using a Quantachrome NOVA 4200e Surface Area and Pore Size analyzer. The Brunauer−Emmett−Teller (BET) method was used to calculate the specific surface area (S_{BET}), while the nonmicroporous surface area ($S_{\neq \mu pores}$) and micropore volume ($V_{\mu pores}$) were determined by the *t*-plot method. Total pore volumes (V_p) were estimated from the amount of N_2 adsorbed at $P/P_0 = 0.98$.

The concentration of acidic sites was determined by acid−base titration, using 200 mg of each material dispersed in 25 mL of NaOH solution (0.02 M) and stirred at room temperature for 48 h.[27] After filtration to separate the solids, the excess OH^- was titrated with a 0.02 M HCl solution using phenolphthalein as an indicator. The acidity was calculated from the difference between the initial NaOH content and the amount determined by titration, normalized to the sample weight.

Surface morphology was examined by scanning electron microscopy (SEM) using an FEI Quanta 400 FEG ESEM/EDAX Genesis X4M instrument equipped with an Everhart−Thornley detector.

High-angle annular dark field scanning transmission electron microscopy (HAADF-STEM) images of Ru/CNT_{ox} were acquired using an FEI Talos F200X microscope operating at 200 kV, equipped with an X-FEG electron source. Particle size distributions were determined by the measurement of 223 nanoparticles, and the average diameter was calculated by $d_M = \frac{\sum d_i n_i}{\sum n_i}$, where n_i is the number of particles with diameter d_i.[28]

Powder X-ray diffraction (XRD) patterns of the catalysts were obtained on a Philips X'Pert MPD diffractometer (Cu−Kα = 0.15406 nm). The diffracted intensity of Cu−Kα radiation was measured in the 2θ range between 5° and 100°.

https://doi.org/10.1021/acssuschemeng.5c12040
ACS Sustainable Chem. Eng. 2026, 14, 4042−4052

Table 1. Textural Properties and Acidity of the Materials

sample	S_{BET} ± 20 (m^2 g^{-1})	$S_{\neq\mu pores}$ ± 10 (m^2 g^{-1})	$V_{\mu pores}$ ± 0.01 (cm^3 g^{-1})	V_p ± 0.01 (cm^3 g^{-1})	acidity ± 0.2 (mmol H^+ g_{cat}^{-1})
CNT	229	229	-	1.53	<0.01
CNT_i	253	253	-	1.44	3.4
CNT_{ox}	291	284	0.01	1.81	1.4
Ru/CNT_{ox}	244	228	0.01	1.67	2.0
HY	667	133	0.25	0.45	3.6
HZSM5	352	21	0.16	0.21	1.8

To determine the particle size distribution, the LDPE was dispersed in an ethanol solution and analyzed using a Beckman Coulter LS320 Laser Diffraction Particle Size Analyzer.

Thermogravimetry analysis was performed on LDPE to verify its thermal stability using a STA 409 PC/4/H Luxx NETZSCH thermal analyzer. The plastic was heated in a N_2 atmosphere from 50 to 900 °C at 10 °C min^{-1}, holding at 900 °C first for 7 min in N_2 and then for 13 min in air.

2.4. Catalysts' Evaluation

The catalytic reactions were performed in a 100 mL batch reactor (Parr Instruments, USA; model HPHT 4598). In a typical run, 5 g of model LDPE and 0.5 g of the catalyst were loaded into the reactor. The system was purged three times with N_2, followed by two purges with H_2. The H_2 pressure was then set to the selected value at room temperature. Once the temperature reached 140 °C, stirring was initiated at 400 rpm, and the reactor was further heated to the desired temperature and maintained for a certain time, from 1 to 4 h. At the end of each run, the reactor was immediately cooled to room temperature. The gaseous products were collected, while the liquid products were extracted using 50 mL of hexane. The reactions performed are described as follows:

(i) Blank experiment (no catalyst) to assess the background performance and CNT_{ox} (support).

(ii) Ru/CNT_{ox} (0.5 g) and combined systems of Ru/CNT_{ox} + HY, Ru/CNT_{ox} + HZSM5, Ru/CNT_{ox} + CNT_{ox} (0.4 g of Ru/CNT_{ox} and 0.1 g of zeolite or CNT_{ox}), and Ru/CNT_{ox} + HY + CNT_{ox} (0.4 g of Ru/CNT_{ox}, 0.05 g of HY, and 0.05 g of CNT_{ox}).

(iii) Screening of reaction conditions aiming to optimize the C_8–C_{16} range, by varying the time (1–4 h), temperature (275–350 °C), H_2 pressure (20–50 bar), and stirring rate (200–500 rpm).

(iv) Conversion of waste plastics (LDPE market plastic bag, LDPE ziplock sample bags, and discarded PP pipet tips) under the optimal conditions.

The hazards and safety requirements of this work are detailed in Section S1–Hazards and Safety (in the Supporting Information).

2.5. Products Analysis

The liquid products were analyzed in a Shimadzu TQ8040-NX gas chromatograph coupled to mass spectrometry (GC–MS) using a ZB-5MS-Plus. A C_7–C_{30} *n*-alkanes external standard mixture was used to calibrate the method for product quantification. Alkane isomers were assumed to have the same calibration factors as their corresponding *n*-alkanes. The gas products, typically in the C_1–C_5 range, were analyzed in a DANI (model 1000) gas chromatograph equipped with a flame ionization detector (GC-FID) by using a ValcoPlot Alumina column.

The conversion (X) was determined as described in eq 1

$$X\ (\%) = \frac{m_{i_{feedstock}} - m_{f_{feedstock}}}{m_{i_{feedstock}}} \quad (1)$$

where $m_{i_{feedstock}}$ is the initial mass of plastic loaded in the reactor. The final feedstock weight ($m_{f_{feedstock}}$) was taken as the total mass of dried solids recovered after the reaction ($m_{total\ dried\ solids}$) minus the catalyst weight ($m_{catalyst}$) (eq 2)

$$m_{f_{feedstock}} = m_{total\ dried\ solids} - m_{catalyst} \quad (2)$$

The yields of nonsolid products were calculated based on mass balances. The liquid yield (Y_{liq}) was determined according to eq 3, and the mass of the liquid products (m_{liquid}) was obtained by weighing the reactor after the reaction and subtracting the mass of the unconverted plastic and catalyst.

$$Y_{liq}\ (\%) = \left(\frac{m_{liquid}}{m_{i_{feedstock}}}\right) \times 100 \quad (3)$$

The gas yield (Y_{gas}) was calculated as the remaining mass fraction not accounted for by solids or liquids (m_{gas}), according to eq 4.

$$Y_{gas}\ (\%) = \left(\frac{m_{gas}}{m_{i_{feedstock}}}\right) \times 100 \quad (4)$$

The selectivity of each product i was determined by dividing the GC peak area of the respective compound by the sum of the areas of all identified peaks (eq 5).

$$S_i\ (\%) = \left(\frac{\text{area of product } i}{\text{total area of identified products in the liquid phase}}\right) \times 100 \quad (5)$$

The iso/n (C_8–C_{16}) ratio was calculated according to eq 6.

$$\text{iso}/n(C_8\text{–}C_{16}) = \frac{\text{total mol of iso } C_8\text{–iso}C_{16}}{\text{total mol of } nC_8\text{–}nC_{16}} \quad (6)$$

Some experiments were performed in duplicate. The standard deviations for the conversion were below 1%, while those for liquid and gas yields were ±3%. The standard deviations for the selectivities in the liquid products (*n*-C_7, *n*-C_8–C_{16}, *n*-C_{17}–C_{24}, and C_{25}^+) were ±1, ±4, <1, and <1%, respectively, while the standard deviation for the iso/n (C_8–C_{16}) ratio was ±1%.

3. RESULTS AND DISCUSSION

3.1. Characterization Results

The textural properties of the catalysts and supports, as well as their corresponding acidities, are summarized in Table 1. CNT-based materials exhibit relatively high S_{BET} and notably elevated V_p, which favors the dispersion of Ru nanoparticles on the support. In addition, their high mesoporosity promotes the hydrogenolysis of large molecules such as LDPE and mitigates intraparticle diffusion limitations. In addition, the oxidative treatment of CNT increased the S_{BET} from 229 to 253 m^2 g^{-1} due to the opening of some tube tips and introduction of defects on the tube side walls, as also reported by Ferreira et al.[29] According to the acidity measurements, the acid treatment facilitated the incorporation of acidic groups onto the CNT surface, increasing the acidity to 3.4 mmol g_{cat}^{-1}. However, the incorporation of oxygenated groups on the surface led to a slight decrease in V_p from 1.53 to 1.44 cm^3 g^{-1}, which can be explained by an increase in affinity between the tube bundles, resulting in a decrease in the free space responsible for the porosity. Sample CNT_{ox} displayed even higher S_{BET} and V_p

https://doi.org/10.1021/acssuschemeng.5c12040
ACS Sustainable Chem. Eng. 2026, 14, 4042–4052

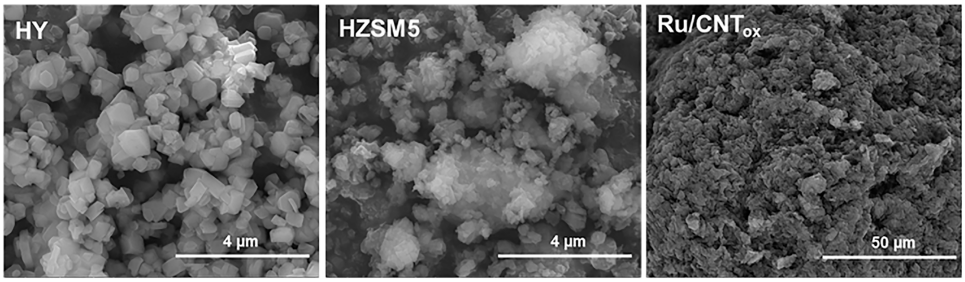

Figure 1. SEM images of HY and HZSM5 (50,000× magnification) and Ru/CNT_{ox} (2000× magnification).

values compared to both CNT and CNT_i, since the thermal treatment under N_2 decomposes oxygenated groups such as carboxylic acids, which is also reflected in the decline in acidity for 1.4 mmol H^+ g_{cat}^{-1}.[30] For the Ru/CNT_{ox} catalyst, the presence of the metallic phase caused a reduction in both S_{BET} and V_p, likely due to partial pore blockage by the deposited Ru nanoparticles. The slight increase in the number of acid sites on the catalyst is consistent with the results of Ribeiro et al.[27] and Ferreira et al.[29] After the metallic phase was impregnated on the CNTs supports, an enhancement in the total number of acid sites was observed, attributed to the increased surface charge on the catalyst surface.

As expected, the HY and HZSM5 zeolites exhibit high microporosity, which is a direct consequence of their well-organized crystalline frameworks. HY shows a BET surface area of 667 m^2 g^{-1}, with 133 m^2 g^{-1} attributable to mesopores, while HZSM5 presents a BET surface area of 352 m^2 g^{-1}, though with a much lower mesoporous contribution (21 m^2 g^{-1}) (Table 1). These results are consistent with the measured micropore volumes of 0.25 and 0.16 cm^3 g^{-1}, respectively. Nevertheless, their total pore volumes are relatively low (0.45 and 0.21 cm^3 g^{-1}), which may hinder the diffusion of large molecules such as LDPE chains, hence restricting the accessibility of the active sites during the reaction. Regarding the acidity, it is observed that the zeolites exhibit high acid site densities, particularly HY (3.6 mmol of H^+ g_{cat}^{-1}), followed by HZSM5 (1.8 mmol of H^+ g_{cat}^{-1}). This behavior confirms the strong acidic nature of these materials, a fundamental characteristic for cracking reactions leading to the C_8−C_{16} hydrocarbon range required for jet fuel production.

SEM images (Figure 1) show the morphology of the zeolites and the Ru/CNT_{ox} catalyst. The HY sample exhibits a block-like morphology, whereas HZSM5 forms aggregates of crystals with predominantly prismatic shapes. Both zeolites display well-defined morphologies with faceted surfaces, consistent with features reported in the literature.[31−33] In contrast, the Ru/CNT_{ox} catalyst shows an irregular surface formed by the entanglement of oxidized carbon nanotubes. SEM analysis revealed no substantial morphological differences between the fresh and spent samples after the first and fourth cycles (Figure S1). The zeolite particles remain well dispersed over Ru/CNT_{ox}, and the overall morphology of both components is maintained, suggesting the absence of severe sintering, collapse of structure, or visible coke deposition under the applied reaction conditions.

HAADF-STEM images (Figure 2) reveal that Ru nanoparticles are homogeneously dispersed over the carbon support. The particle size distribution indicates Ru particle diameters in the range of 0.5−2.8 nm, with an average of approximately 1.2 nm. These results demonstrate the

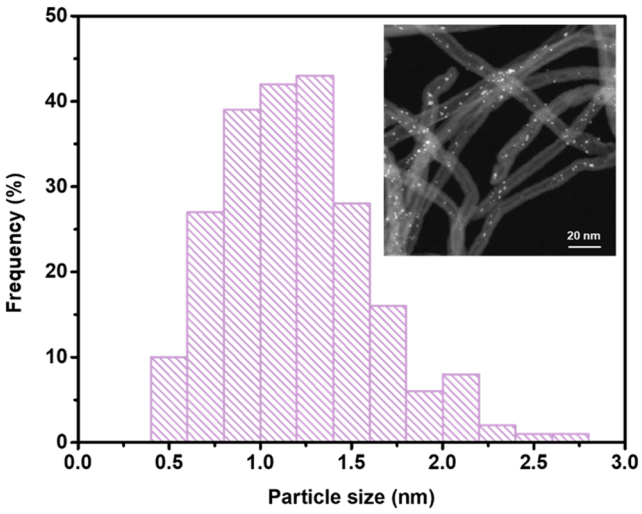

Figure 2. HAADF-STEM image of Ru/CNT_{ox} and Ru particle distribution.

effectiveness of the incipient wetness impregnation method in producing highly dispersed Ru nanoparticles.

To complement the characterization of the studied materials, XRD analysis was carried out in order to investigate the crystalline portion of the catalysts (Figure 3). The XRD

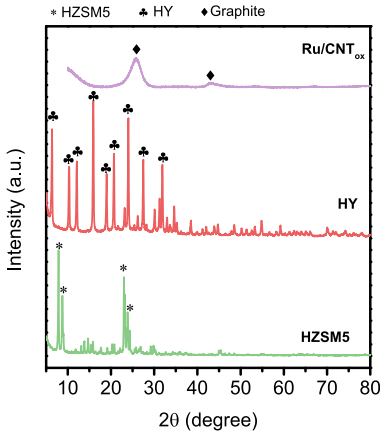

Figure 3. XRD patterns of the materials.

pattern of the HY zeolite exhibits sharp and well-defined diffraction peaks that are characteristic of the faujasite crystalline structure (PDF # 01−077−1551). In the case of HZSM5, the diffractogram displays intense and well-resolved reflections assigned to the mordenite framework inverted (MFI) topology, which confirms the high crystallinity of the

https://doi.org/10.1021/acssuschemeng.5c12040
ACS Sustainable Chem. Eng. 2026, 14, 4042−4052

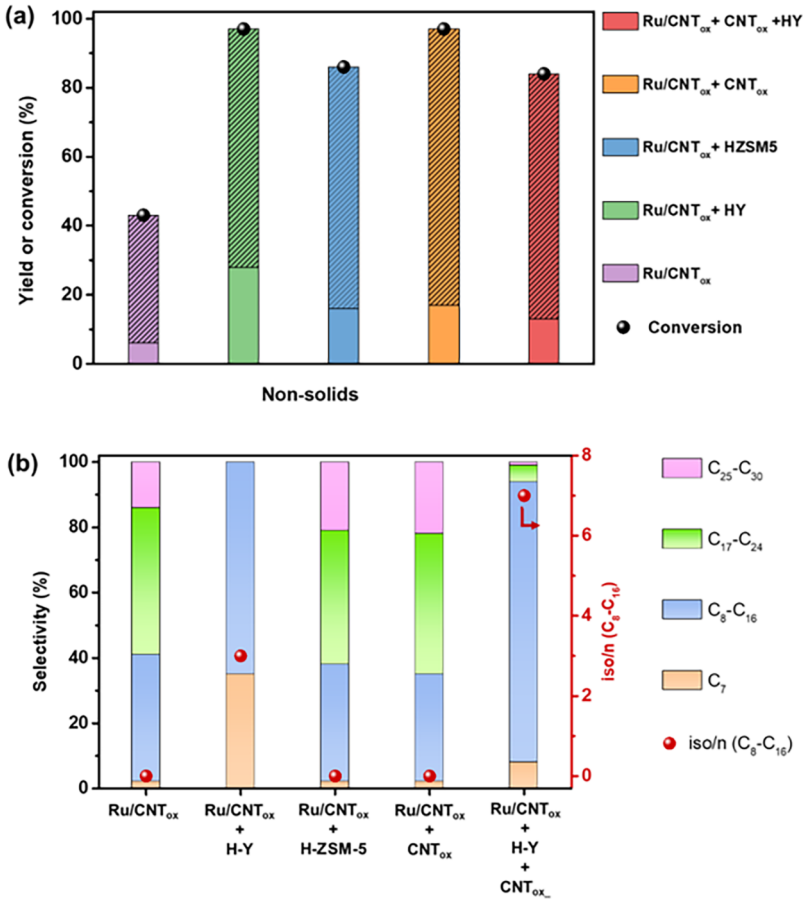

Figure 4. Catalytic screening of Ru/CNT_{ox} and combined systems. (a) Conversion (black dots) and nonsolids yield: liquid (solid bars) and gas (striped bars); (b) liquid products selectivities (bars) and iso/*n* (C_8−C_{16}) ratio (red dots). Reaction conditions: 0.5 g of catalyst, 4 h, 300 °C, 40 bar of initial H_2 pressure, and 400 rpm.

material and the preservation of its structural framework (PDF #44−0003).[34] In contrast, the Ru/CNT_{ox} catalyst displays broad diffraction bands centered at 2θ = 26° and 43°, associated with the (002) and (100) planes of graphitic carbon in carbon nanotubes, respectively (PDF #03−065−6212). The absence of well-defined reflections of Ru species suggests either high dispersion of Ru nanoparticles and/or that the metal loading is below the XRD detection limit. According to the XRD pattern shown in Figure S2, the characteristic crystalline phases of both the zeolite and the carbon-supported catalyst were preserved after the first catalytic run, indicating that no significant structural degradation occurred.

In regard to LDPE, particle size analysis showed that the plastic had a specific surface area of 147 $cm^2\ g^{-1}$ and an average particle size of 441 μm. Relatively to the size distribution, it was possible to determine d_{10} = 300.4 ± 1.6 μm, d_{50}= 428.3 ± 0.6 μm, and d_{90}= 587.4 ± 0.9 μm, indicating that 10%, 50%, and 90% of the particles have diameters below those values, respectively.

The plastic granules were also analyzed by thermogravimetric analysis (TGA) to obtain the mass-loss curve as a function of temperature (Figure S3). This analysis is relevant since the catalytic tests are carried out under high-temperature conditions. Mass loss under an inert atmosphere began at approximately 390 °C, whereas the catalytic experiments were conducted at lower temperatures.

3.2. Catalytic Performance

To assess the conversion of LDPE into aviation fuel-range hydrocarbons, several catalytic tests were performed. Initially, a blank experiment and a test with the carbon support alone were conducted, and the results are summarized in Table S1. As expected, low conversions were achieved, 6% for the blank and 2% for CNT_{ox}. In both cases, LDPE was mainly converted into gases.

Subsequently, screening tests with Ru/CNT_{ox} and the combined catalytic systems were performed. The results are presented in Figure 4, and the corresponding numerical values are provided in Table S2. According to Figure 4a, the Ru/CNT_{ox} catalyst alone was not sufficient to fully convert the LDPE, producing mainly gas products (37%). To enhance the catalytic activity, this catalyst was combined with different zeolites as well as CNT_{ox}. By the outcomes, the presence of an extra acid solid increased the conversion and, consequently, the yield of nonsolid products. The density of acid sites played a critical role, influencing the selectivity in liquid products, as shown in Figure 4b. The Ru/CNT_{ox} + HZSM5 and Ru/CNT_{ox} + CNT_{ox} systems exhibited similar total acid site densities (see Table 1) and comparable product distributions in the liquid phase: 33−36% C_8−C_{16}, 41−43% C_{17}−C_{24}, and 21−22% >C_{24} products. The systems with higher acid site density, such as Ru/CNT_{ox} + HY and Ru/CNT_{ox} + CNT_{ox} + HY, were interesting in terms of jet fuel-range selectivity (65 and 86%, respectively). Increasing the acidity facilitated both the

https://doi.org/10.1021/acssuschemeng.5c12040
ACS Sustainable Chem. Eng. 2026, 14, 4042−4052

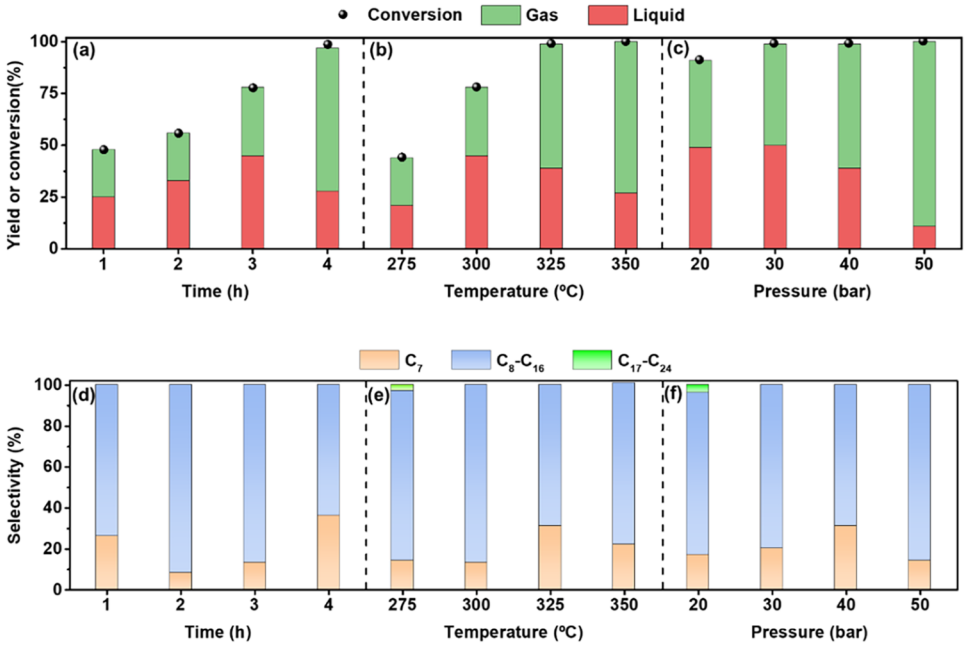

Figure 5. Effect of temperature, reaction time, and initial H_2 pressure on product distribution. Reaction conditions: (a, d) 0.4 g Ru/CNT_{ox} + 0.1 g HY, 300 °C, 1−4 h, 40 bar of initial H_2 pressure and 400 rpm; (b, e) 0.4 g Ru/CNT_{ox} + 0.1 g HY, 275−350 °C, 3 h, 40 bar of initial H_2 pressure and 400 rpm; (c, f) 0.4 g Ru/CNT_{ox} + 0.1 g HY, 325 °C, 3 h, 20−50 bar of initial H_2 pressure and 400 rpm.

cracking of large molecules into small ones and the formation of more C_8−C_{16} isomers. Although the Ru/CNT_{ox} + CNT_{ox} + HY system exhibited the highest selectivity toward jet fuel-range hydrocarbons, the Ru/CNT_{ox} + HY mixture achieved higher overall conversion and liquid yield (97 and 28%, respectively) compared to those obtained with Ru/CNT_{ox} + CNT_{ox} + HY (84 and 13%, respectively). This enhanced liquid yield highlights the superior overall efficiency of the Ru/CNT_{ox} + HY system, despite its lower C_8−C_{16} selectivity.

In order to enhance liquid yields and improve selectivity toward aviation fuel components, the reaction conditions were optimized by using the Ru/CNT_{ox} + HY system. The outcomes of nonsolids yields, conversion, and liquid product selectivities obtained under different temperatures, reaction times, and initial H_2 pressures are compiled in Figure 5. For the sake of clarity, the results referring to each parameter are detailed in Table S3.

According to Figure 5a, the liquid yield increased with reaction time, reaching 45% at 3 h, but then sharply decreased to 28% at 4 h. The selectivity toward the aviation fuel range followed a similar trend, dropping to 64% at 4 h (Figure 5d), indicating that cracking reactions leading predominantly to gaseous products and C_7 hydrocarbons become dominant beyond that point. From 2 to 3 h of reaction, the C_8−C_{16} selectivity remained practically the same (taking into account the experimental error for this hydrocarbon range). However, at 3 h, the global liquid yield reached the maximum value (45%). Therefore, 3 h was determined to be the optimal reaction time.

Temperature also played a decisive role in LDPE conversion to liquid and gaseous products as well as in product selectivity (Figure 5b,e). The global liquid yield increased up to 300 °C, reaching a maximum of 45%. At 350 °C, the gas yield rose to 73%, indicating that higher temperatures favored cracking reactions. Regarding C_8−C_{16} selectivity, it was 87% at 300 °C and decreased to 69% at 325 °C. However, the conversion at 325 °C was significantly higher (99%) compared to 300 °C (78%). Although the liquid yield was slightly lower at 325 °C, this temperature was selected for subsequent experiments, since it ensured an almost complete conversion of the feedstock, enabling full valorization of LDPE.

As shown in Figure 5c, hydrocracking became more pronounced at higher pressures (40−50 bar), promoting gas formation. At 50 bar, the gas yield reached a maximum of 89%. On the other hand, the selectivity toward C_8−C_{16} hydrocarbons (Figure 5f) remained nearly constant between 20 and 30 bar (approximately 80%). However, C_{17}−C_{24} compounds were still present at 20 bar (4%). Therefore, 30 bar was identified as the optimal pressure, as it maximized selectivity in the desired range while minimizing heavier fractions.

Finally, to confirm that the reactions occur under kinetic control, different stirring rates (200−500 rpm) were tested. No significant variations in conversion or selectivity were observed (Table S4), confirming that the catalytic system was not limited by external mass transfer. While external mass transfer limitations were excluded through stirring rate variation experiments, it is worth noting that internal diffusion within the zeolite micropores and the CNT structure can also influence product selectivity. In bifunctional hydrocracking systems, limited internal diffusion can prolong the residence times of intermediates in acidic sites, leading to secondary cracking and increased gas formation. Conversely, the open structure of CNTs can facilitate rapid transport of larger intermediates, potentially contributing to the high selectivities in the range C_8−C_{16} observed in this study. Although a detailed analysis of internal diffusion was beyond the scope of this work, these effects may partially explain the observed differences among the various zeolite combinations.

Based on the catalytic results shown in Figures 4 and 5, it can be concluded that LDPE conversion into fuel-range hydrocarbons proceeds through sequential reaction pathways enabled by the bifunctional nature of the Ru/CNT_{ox} + HY

https://doi.org/10.1021/acssuschemeng.5c12040
ACS Sustainable Chem. Eng. 2026, 14, 4042−4052

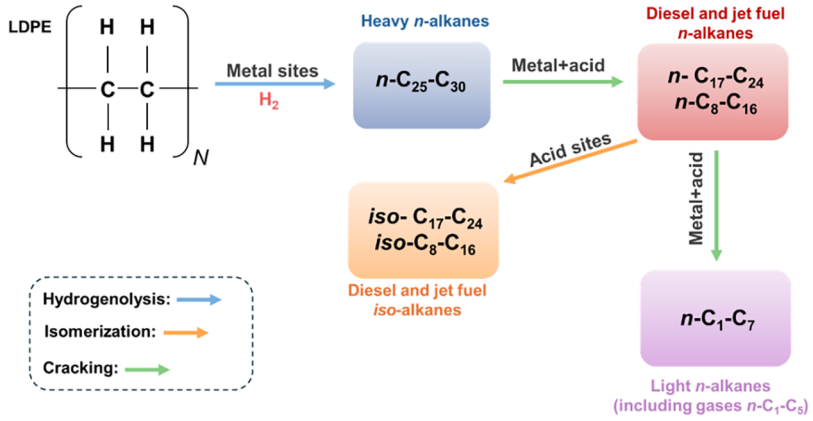

Figure 6. Proposed reaction pathways for LDPE conversion into fuels over Ru/CNT_{ox} + HY.

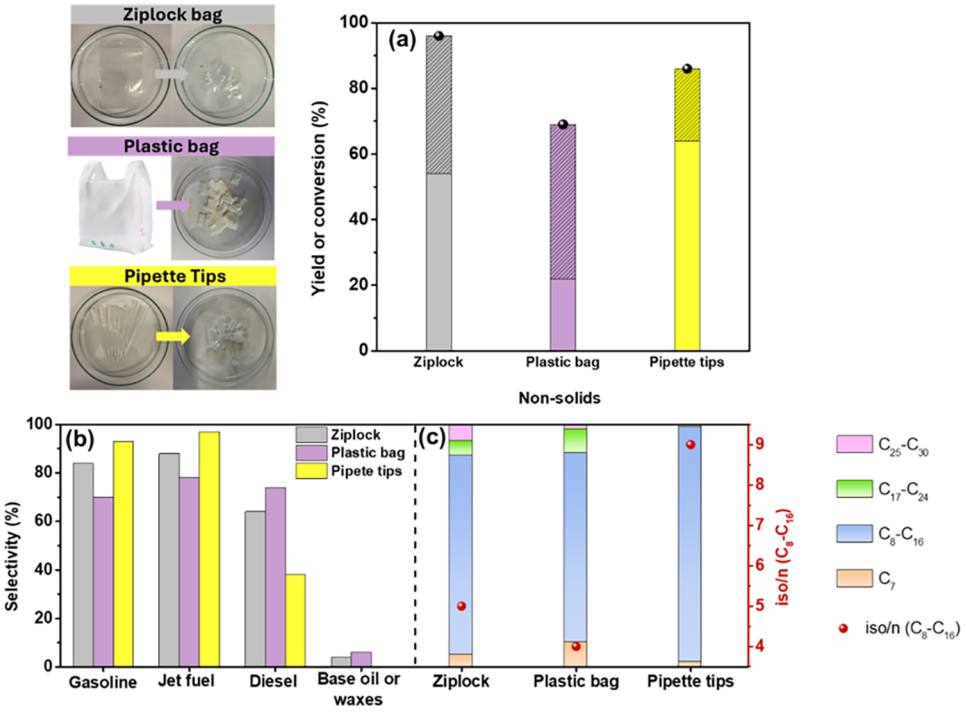

Figure 7. Conversion of different plastics into fuels. (a) Conversion (black dots) and nonsolids yield: liquid (solid bars) and gas (striped bars); (b) selectivities by fuel range: gasoline (C_5−C_{12}), jet fuel (C_8−C_{16}), diesel (C_9−C_{22}), base oil/waxes (C_{20}−C_{30}); (c) liquid product selectivities (from C_7 to C_{30}) and iso/*n* (C_8−C_{16}) ratio (red dots). Reaction conditions: 0.4 g of Ru/CNT_{ox} and 0.1 g of HY, 325 °C, 3 h of reaction, 30 bar of initial H_2 pressure, and 400 rpm.

system (Figure 6). Initially, H_2 is dissociatively adsorbed on the Ru metallic sites. The LDPE polymer chains then interact with these active sites, where C−C bond cleavage occurs via hydrogenolysis, generating long-chain saturated intermediates (*n*-C_{25}−C_{30}). These intermediates are subsequently transferred mainly to the Brønsted acid sites of the HY zeolite (and to a minor extent to the CNT_{ox} support), where they undergo cracking into smaller chains in the *n*-C_{17}−C_{24} and *n*-C_8−C_{16} ranges. The HY zeolite then plays a crucial role in promoting isomerization reactions, leading to the formation of branched hydrocarbons that are essential for jet fuel properties. Excessive cracking of shorter chains, favored at higher H_2 pressures through metal-acid cracking pathways, ultimately generates light alkanes (C_1−C_7). This mechanism aligns with previous studies employing Ru-based catalysts.[8,16,35] However, the present mechanism differs from the one proposed by Wang et al.,[21] which also studied a combined system of Pt/WO_3/ZrO_2 + HY. The authors proposed that cracking on zeolite occurs first, producing olefins that are subsequently hydrogenated in the metal sites. In the present work, the reaction preferentially begins with hydrogenolysis on Ru/CNT_{ox}, followed by cracking and isomerization over HY. This preference is attributed to the higher proportion of Ru relative to the zeolite in the catalytic system, which drives the reaction pathway more selectively toward C_8−C_{16} hydrocarbons. Overall, these findings highlight that the metal-acid balance is a decisive factor in controlling the reaction pathway and final product selectivity.

Recyclability tests with Ru/CNT_{ox} + HY were performed to assess the stability of the catalytic system, in which four runs were performed under the same conditions. After each cycle, the catalyst was recovered by filtration, properly washed several

https://doi.org/10.1021/acssuschemeng.5c12040
ACS Sustainable Chem. Eng. 2026, 14, 4042−4052

Table 2. Comparison of the Results with Those Reported in the Literature for the Conversion of Polyolefins into Liquid Fuels

reference	substrate	catalyst	catalyst:substrate ratio	reaction conditions	solvent	results
7	HDPE	5 wt % Ru/C	1:5	220 °C, 1 h, 60 bar	*n*-hexane	X = 99% S_{C8-C16} = 60% $S_{C17-C22}$ = 10%
17	LDPE	1 wt % Pt/Al-MCM-48	1:10	300 °C, 4 h, 40 bar	-	X = 99.3% S_{C1-C8} = 8.9% S_{C9-C15} = 85.9% $S_{C16-C21}$ = 4.5%
13	HDPE	H-USY (Si/Al = 15)	1:4	300 °C, 1 h, 20 bar	-	X = 60% S_{C7-C12} = 48% $S_{C13-C20}$ = 50%
18	LDPE	1 wt % Ru/milled-ZSM-22	1:10	290 °C, 2 h, 50 bar	-	Maximum liquid products of 80.7%
9	HDPE	Ni- Hβ	3:4	250 °C, 20 h, 30 bar	-	X = 95% S_{C8-C16} = 80%
8	LDPE	5 wt % Ru/C	1:28	200 °C, 16 h, 20 bar	*n*-octadecane	X = 100% Liquid products yield of 45%
16	PE	5 wt % Ru/C	1:10	175 °C, 76 h, 82 bar	-	X = 100% [a]$S_{C12-C20}$ = 57%
10	LDPE, HDPE and PP	5 wt % Ru/CeO_2	1:3.4 or 1:6.8	240 °C, 8- 72 h, 60 bar	-	X = 99% Liquid products yield around 80%
22	LDPE	0.5 wt % Pt/WO_3/ZrO_2 + HY (Si/Al = 16)	1:10	250 °C, 1 h, 30 bar	-	X = 100% [a]S_{C5-C7} = 52% [a]S_{C8-C16} = 31% [a]S_{C1-C4} = 9%
35	LDPE	5%Ru/15WZR	1:40	250 °C, 2 h, 50 bar	-	X = 99% [a]S_{C5-C12} = 25% [a]S_{C8-C16} = 33% [a]S_{C9-C22} = 47%
38	LDPE	5%Ni/SiO_2	1:5	280 °C, 4 h, 30 bar	-	X = 100% S_{C5-C22} = 81.2%
21	LDPE	Pt−Ru/TMSN + H-β (Si/Al = 30)	1:5	260 °C, 2 h, 10 bar	-	X = 100% S_{C4-C8} = 75.6%
this work	LDPE	2.5%Ru/CNT_{ox} + HY (Si/Al = 24)	1:10	325 °C, 3 h, 30 bar	-	X = 99% S_{C8-C16} = 80% iso/n = 4
this work	Residues(LDPE and PP)	2.5%Ru/CNT_{ox} + HY (Si/Al = 24)	1:10	325 °C, 3 h, 30 bar	-	X = 86−96% S_{C8-C16} = 80−90% iso/n = 4−9

[a]Molar selectivity determined as S_i (%) = $\left(\frac{\text{mol of C of product } i}{\text{mol of C of total quantified products}}\right) \times 100$.

times with acetone, and dried overnight in an oven at 110 °C for the next catalytic run. According to Table S5, from the second reaction cycle onward, heavier compounds (C_{17}−C_{30}) began to form, indicating a slight decrease in catalytic cracking activity. However, selectivity remains stable in C_8−C_{16} (80% at the end of cycle 1 and 78% at the end of cycle 4). These results demonstrate the excellent stability of the Ru/CNT_{ox} and HY catalyst system.

Having identified the optimal conditions with LDPE, we next evaluated the catalyst's performance on postconsumer real plastic waste feedstocks to assess practical applicability. The catalytic conversion results of a ziplock bag of LDPE, a used plastic bag of LDPE with 80% recycled content, and used pipet tips of PP are presented in Figure 7. The detailed numerical data are listed in Tables S6 and S7. According to Figure 7a, both the ziplock bag and the pipet tips provided a high yield of liquid products after the reaction, since LDPE and PP have high thermal stability, and their hydroprocessing generally produces hydrocarbons in the jet fuel and diesel range.[36] Regarding the plastic bag, its lower conversion and reduced yield of liquid hydrocarbons may be related to the fact that it consists of approximately 80% recycled material, which probably contains additives incorporated during previous manufacturing processes. These additives may promote the formation of gaseous products rather than liquids. Overall, the liquid products distribution is among the gasoline (C_5−C_{12}), jet fuel (C_8−C_{16}), and diesel range (C_9−C_{22}), with a little fraction of base oil/waxes (C_{20}−C_{30}) (Figure 7b). This trend is particularly evident for the PP-derived feedstock (pipet tips), which exhibited not only a higher selectivity in jet fuel but also a significantly greater iso/n C_8−C_{16} ratio compared to LDPE-based samples (Figure 7c). The presence of tertiary carbon atoms in the PP molecular structure facilitates the formation of stable tertiary intermediates during hydroprocessing, which results in more chain rearrangements and a higher degree of isomerization, by the formation of a carbenium ion.[21,37]

https://doi.org/10.1021/acssuschemeng.5c12040
ACS Sustainable Chem. Eng. 2026, 14, 4042−4052

3.3. Comparison with Other Works

In recent years, numerous studies have investigated the production of fuels from plastics, using both model polymers and postconsumer waste as feedstocks to provide a more sustainable end-of-life for these materials. For the model LDPE feed, the bifunctional catalyst system Ru/CNT_{ox} + HY at 325 °C and 30 bar of H_2 delivered a high selectivity to the jet fuel range (around 80%) in the liquid phase with an iso/*n* ratio of 4. These results agree well with the performances reported by Zhao et al.[38] using Ni/SiO_2 (S_{C5-C22} = 81.2%) and by Cheng et al.[18] using Ru/milled-ZSM-22 (liquid product yield of 80%). Compared to Liu,[17] who reported 85.9% selectivity in the liquid phase for the C_9-C_{15} range with Pt/Al-MCM-48 at 300 °C, the present system required a slightly higher reaction temperature but achieved a similar distribution of liquid fractions, with the added advantage of significant isomerization in the C_8-C_{16} range.

Relative to studies employing zeolitic catalysts, such as Costa et al.[13] with H-USY (Si/Al = 15), which yielded balanced gasoline and diesel fractions at 300 °C and 60% conversion, the combined Ru/CNT_{ox} + HY system exhibited higher conversion and narrower liquid distribution in the jet fuel range. In addition, the balance in the proportion of Ru/CNT_{ox} and HY in this work was crucial to reducing the degree of hydrocracking reactions. Conversely, Liu et al.[22] and Wang et al.[21] reported a higher selectivity toward gasoline-range products in their combined Pt- or Ru-based catalyst-zeolite systems. These findings suggest that the acid functionality of HY, combined with the hydrogenation activity of Ru/CNT_{ox}, effectively promotes moderate chain cracking. The balance between these two functions distinguishes this system from those that favor excessive cracking to produce gases or form wax products.

When applied to real waste plastics (LDPE and PP), the optimized conditions provided liquid selectivities of 80−90% in the jet fuel range, with iso/*n* ratios between 4 and 9. In addition, LDPE and PP wastes were converted into 54 and 64% total liquids, respectively, after only 3 h of reaction. In comparison, Nakaji et al.[10] obtained up to 87% liquid yield from mixed plastic feeds using Ru- and Pt-based catalysts, but their experiments required significantly longer reaction times (8−72 h) and higher H_2 pressure (60 bar). The higher iso/*n* ratios observed in this work are particularly notable for PP-derived products, reflecting PP's greater propensity to form tertiary carbocations that promote chain rearrangements and isomerization. Overall, compared with the studies summarized in Table 2, the present system demonstrates competitive or superior liquid yields and a higher degree of molecular branching, both desirable for producing hydrocarbon fuels with improved combustion properties. In this context, the proposed catalytic system stands out due to its ability to selectively produce high-quality jet fuel-range hydrocarbons under solvent-free and relatively mild conditions (325 °C, 3 h, 30 bar H_2), achieving a 50% liquid yield, of which 80% corresponds to C_8-C_{16} hydrocarbons. Moreover, this catalytic system also provides a significant degree of isomerization (iso/*n* = 4−9) and demonstrates high conversion and robustness toward real plastic residues.

4. CONCLUSIONS

In this study, a systematic screening of Ru/CNT_{ox} combined with different solid acids (HY, HZSM5, and CNT_{ox} itself) was performed for the conversion of model LDPE into hydrocarbons in the jet fuel range under the standard reaction conditions of 300 °C, 40 bar initial H_2 pressure, and 4 h of reaction. The Ru/CNT_{ox} + CNT_{ox} + HY and Ru/CNT_{ox} + HY catalytic systems exhibited the best performance, achieving full conversion and high selectivity to the desired fraction, mainly due to the higher acid site densities. Under the optimized conditions (325 °C, 30 bar of initial H_2 pressure and 3 h of reaction), the Ru/CNT_{ox} + HY system exhibited the best performance in terms of conversion (99%), global liquid yield (50%), and jet-fuel selectivity in the liquid products (80%). In contrast, optimization studies revealed that prolonging the reaction time to 4 h, as well as increasing the H_2 pressure and temperature, promoted hydrocracking reactions, favoring gas formation.

When applied to real waste plastics, the optimized Ru/CNT_{ox} + HY system maintained an excellent catalytic activity. For plastic bag and Ziplock residues (both LDPE-based), the conversion ranged from 69 to 96%, with liquid yields of 22−54%, jet fuel-range selectivities in the liquid phase of 78−82%, and iso/*n* (C_8-C_{16}) ratios between 4 and 5. In the case of PP waste, the conversion, liquid yield, jet fuel selectivity in the liquid products, and iso/*n* (C_8-C_{16}) ratio were 86, 64, 97, and 9 %, respectively. The higher degree of isomerization observed for PP-derived products emphasizes the influence of the polymer structure on product selectivity. These values are comparable to or exceed those reported in the literature while requiring shorter reaction times and yielding narrower hydrocarbon distributions.

Overall, the Ru/CNT_{ox} + HY catalytic system demonstrated robustness and versatility in converting both model and real plastics into high-quality liquid fuels, highlighting its potential for sustainable plastic waste valorization strategies.

■ ASSOCIATED CONTENT

Data Availability Statement

The original contributions presented in the study are included in the article/Supporting Information, and any further inquiries can be directed to the corresponding author.

Supporting Information

The Supporting Information is available free of charge at https://pubs.acs.org/doi/10.1021/acssuschemeng.5c12040.

Additional information on hazards and safety; TGA analysis of commercial LDPE; catalytic results of blank and support experiments; results referred to catalytic screening; results referred to reaction conditions optimization; catalytic results of the effect of the stirring rate; results referred to the catalytic conversion of the ziplock, plastic bag, and pipet tips (PDF)

■ AUTHOR INFORMATION

Corresponding Author

Lucília S. Ribeiro − *LSRE-LCM, ALiCE, Faculty of Engineering, University of Porto, 4200-465 Porto, Portugal;* orcid.org/0000-0003-0506-6183; Email: lucilia@fe.up.pt

Authors

Karoline Kaiser Ferreira − *LSRE-LCM, ALiCE, Faculty of Engineering, University of Porto, 4200-465 Porto, Portugal*

https://doi.org/10.1021/acssuschemeng.5c12040
ACS Sustainable Chem. Eng. 2026, 14, 4042−4052

Mariana Rita Tuna Oliveira Costa − *LSRE-LCM, ALiCE, Faculty of Engineering, University of Porto, 4200-465 Porto, Portugal*

José J. M. Órfão − *LSRE-LCM, ALiCE, Faculty of Engineering, University of Porto, 4200-465 Porto, Portugal;* orcid.org/0000-0003-3098-8032

Manuel Fernando R. Pereira − *LSRE-LCM, ALiCE, Faculty of Engineering, University of Porto, 4200-465 Porto, Portugal;* orcid.org/0000-0002-5447-2471

Complete contact information is available at: https://pubs.acs.org/10.1021/acssuschemeng.5c12040

Author Contributions

†K.K.F. and M.R.T.O.C. contributed equally to this work.

Notes

The authors declare no competing financial interest.

■ ACKNOWLEDGMENTS

This work was supported by national funds through the FCT/MECI, under the project Waste2Jet - Food Waste Catalytic Valorisation into Eco-Friendly Aviation Fuels: A Pathway for Sustainable Air Transportation with reference 2024.14180.PEX and with DOI 10.54499/2024.14180.PEX. This work was also financially supported by Fundação para a Ciência e a Tecnologia, I.P./MECI through national funds: LSRE-LCM, UID/50020/2025 (10.54499/UID/50020/2025); and ALiCE, LA/P/0045/2020 (10.54499/LA/P/0045/2020). K.K.F. acknowledges her Ph.D. scholarship (DOI: 10.54499/2022.12949.BD) from FCT. The authors also show gratitude to CEMUP for the assistance with SEM analyses. L.S.R. and M.F.R.P. are members of the CYTED BioFuturo network (424RT0157).

■ REFERENCES

(1) Cabrera, E.; de Sousa, J. M. M. Use of Sustainable Fuels in Aviation—A Review. *Energies* **2022**, *15* (7), No. 2440.

(2) Meegoda, J. N.; Pennock, W. H.; Brenckman, C.; Borgaonkar, A. D. Would the Oceans Become Toxic to Humanity Due to Use and Mismanagement of Plastics? *Int. J. Environ. Res. Public Health* **2025**, *22* (1), No. 17.

(3) Houssini, K.; Li, J.; Tan, Q. Complexities of the Global Plastics Supply Chain Revealed in a Trade-Linked Material Flow Analysis. *Commun. Earth Environ.* **2025**, *6* (1), No. 257.

(4) Pilapitiya, P. G. C. N. T.; Ratnayake, A. S. The World of Plastic Waste: A Review. *Cleaner Mater.* **2024**, *11*, No. 100220.

(5) Chanda, M. Chemical Aspects of Polymer Recycling. *Adv. Ind. Eng. Polym. Res.* **2021**, *4* (3), 133−150.

(6) Kwon, T.; Ahn, B.; Kang, K. H.; Won, W.; Ro, I. Unraveling the Role of Water in Mechanism Changes for Economically Viable Catalytic Plastic Upcycling. *Nat. Commun.* **2024**, *15* (1), No. 10239.

(7) Jia, C.; Xie, S.; Zhang, W.; Intan, N. N.; Sampath, J.; Pfaendtner, J.; Lin, H. Deconstruction of High-Density Polyethylene into Liquid Hydrocarbon Fuels and Lubricants by Hydrogenolysis over Ru Catalyst. *Chem. Catal.* **2021**, *1* (2), 437−455.

(8) Rorrer, J. E.; Beckham, G. T.; Román-Leshkov, Y. Conversion of Polyolefin Waste to Liquid Alkanes with Ru-Based Catalysts under Mild Conditions. *JACS Au* **2021**, *1* (1), 8−12.

(9) Zhang, G.; Mao, Q.; Yue, Y.; Gao, R.; Duan, Y.; Du, H. Ni-Based Catalysts Supported on Hbeta Zeolite for the Hydrocracking of Waste Polyolefins. *RSC Adv.* **2024**, *14* (23), 15856−15861.

(10) Nakaji, Y.; Tamura, M.; Miyaoka, S.; Kumagai, S.; Tanji, M.; Nakagawa, Y.; Yoshioka, T.; Tomishige, K. Low-Temperature Catalytic Upgrading of Waste Polyolefinic Plastics into Liquid Fuels and Waxes. *Appl. Catal., B* **2021**, *285*, No. 119805.

(11) Azam, M. U.; Vete, A.; Afzal, W. Process Simulation and Life Cycle Assessment of Waste Plastics: A Comparison of Pyrolysis and Hydrocracking. *Molecules* **2022**, *27* (22), No. 8084.

(12) Geerts, L.; Ramachandran, R. K.; Dendooven, J.; Radhakrishnan, S.; Seo, J. W.; Detavernier, C.; Martens, J.; Sree, S. P. Creation of Gallium Acid and Platinum Metal Sites in Bifunctional Zeolite Hydroisomerization and Hydrocracking Catalysts by Atomic Layer Deposition. *Catal. Sci. Technol.* **2020**, *10* (6), 1778−1788.

(13) Costa, C. S.; Ribeiro, M. R.; Silva, J. M. Catalyst Accessibility and Acidity in the Hydrocracking of HDPE: A Comparative Study of H-USY, H-ZSM-5, and MCM-41 Modified with Ga and Al. *Molecules* **2024**, *29* (17), No. 4248.

(14) Yadav, M. D.; Joshi, H. M.; Sawant, S. V.; Dasgupta, K.; Patwardhan, A. W.; Joshi, J. B. Advances in the Application of Carbon Nanotubes as Catalyst Support for Hydrogenation Reactions. *Chem. Eng. Sci.* **2023**, *272*, No. 118586.

(15) Ferreira, K. K.; Magalhães, B. F. O.; Ribeiro, L. S.; Pereira, M. F. R. Co−Mo Catalysts Supported on CNT/H-ZSM-5 Composites for Selective Production of Sustainable Aviation Fuel-Range Alkanes. *Energy Fuels* **2025**, *39* (30), 14615−14626.

(16) Chen, L.; Zhu, Y.; Meyer, L. C.; Hale, L. V.; Le, T. T.; Karkamkar, A.; Lercher, J. A.; Gutiérrez, O. Y.; Szanyi, J. Effect of Reaction Conditions on the Hydrogenolysis of Polypropylene and Polyethylene into Gas and Liquid Alkanes. *React. Chem. Eng.* **2022**, *7* (4), 844−854.

(17) Liu, Y. Hydrocracking of Polyethylene to Jet Fuel Range Hydrocarbons over Bifunctional Catalysts Containing Pt- and Al-Modified MCM-48. *Reactions* **2020**, *1* (2), 195−209.

(18) Cheng, L. L.; Chen, R. Z.; Zhu, W. Q.; Tian, S. N.; Gu, J.; Yuan, H. R.; Chen, Y. Parameter Selection for the Hydroconversion of Waste Polyethylene Plastic under Mild Conditions: A Comprehensive Evaluation. *Sci. China Technol. Sci.* **2024**, *67* (8), 2413−2426.

(19) Choi, I. H.; Lee, H. J.; Rhim, G. B.; Chun, D. H.; Lee, K. H.; Hwang, K. R. Catalytic Hydrocracking of Heavy Wax from Pyrolysis of Plastic Wastes Using Pd/Hβ for Naphtha-Ranged Hydrocarbon Production. *J. Anal. Appl. Pyrolysis* **2022**, *161*, No. 105424.

(20) Wu, X.; Liu, X.; Song, Y.; Liu, W.; Deng, R.; Chu, X.; Song, S.; Zhang, H.; Wang, X. A Minimalist Design for a Dual-Catalyst System for High-Efficiency Conversion of Waste Plastics into Liquid Fuel Products. *J. Am. Chem. Soc.* **2025**, *147* (25), 21907−21915.

(21) Wang, W.; Wang, S.; Li, W.; Lv, Y.; Cao, Z.; Wang, X.; Wang, C.; Chen, G.; Wang, R.; Jiang, Y.; Li, C.; Gao, D. Coordinating Cracking and Hydrogenation of Polyethylene Waste via Acid-Metal Site Isolation for Selective Hydrocarbon Production. *Chem. Eng. Sci.* **2025**, *315*, No. 121882.

(22) Liu, S.; Kots, P. A.; Vance, B. C.; Danielson, A.; Vlachos, D. G. Plastic Waste to Fuels by Hydrocracking at Mild Conditions. *Sci. Adv.* **2021**, *7*, 8283−8304.

(23) Wang, S.; Wang, W.; Chu, M.; Gao, D.; Wang, Y.; Lv, Y.; Wang, R.; Song, L.; Zhao, H.; Chen, J.; Chen, G. Ultra-Narrow Alkane Product Distribution in Polyethylene Waste Hydrocracking by Zeolite Micro-Mesopore Diffusion Optimization. *Angew. Chem., Int. Ed.* **2024**, *63* (49), No. e202409288, DOI: 10.1002/anie.202409288.

(24) Han, W.; Lin, L.; Cen, Z.; Ke, Y.; Xu, Q.; Zhu, J.; Mei, X.; Xia, Z.; Zheng, X.; Wang, Y.; Liu, Y.; He, M.; Wu, H.; Han, B. One-Pot Catalytic Conversion of Polyethylene Wastes to Gasoline through a Dual-Catalyst System. *Chem* **2025**, *11* (2), No. 102340.

(25) Ali, S. S.; Zamir, S.; Raheman, A. R. S.; Ansari, K. B.; Qyyum, M. A.; Al Mesfer, M. K.; Danish, M.; Khan, M. S.; Al-Muhtaseb, A. H. Current Progress in Thermochemical Conversion of Plastics into Jet-Fuel Hydrocarbons and Recommendations for COVID-19 Waste Management. *Process Saf. Environ. Prot.* **2022**, *166*, 535−557.

(26) Figueiredo, J. L.; Pereira, M. F. R.; Freitas, M. M. A.; Órfão, J. J. M. Modification of the Surface Chemistry of Activated Carbons. *Carbon* **1999**, *37*, 1379−1389.

(27) Ribeiro, R. S.; Silva, A. M. T.; Figueiredo, J. L.; Faria, J. L.; Gomes, H. T. Removal of 2-Nitrophenol by Catalytic Wet Peroxide Oxidation Using Carbon Materials with Different Morphological and Chemical Properties. *Appl. Catal., B* **2013**, *140−141*, 356−362.

(28) Ribeiro, L. S.; Órfão, J. J. M.; Pereira, M. F. R. Enhanced Direct Production of Sorbitol by Cellulose Ball-Milling. *Green Chem.* **2015**, *17* (5), 2973−2980.
(29) Ferreira, K. K.; Di Stasi, C.; Ayala-Cortés, A.; Ribeiro, L. S.; Pinilla, J. L.; Suelves, I.; Pereira, M. F. R. Hydroprocessing of Waste Cooking Oil to Produce Liquid Fuels over Ni-Mo and Co-Mo Supported on Carbon Nanotubes. *Biomass Bioenergy* **2024**, *191*, No. 107480.
(30) Ribeiro, L. S.; Delgado, J. J.; Órfão, J. J. M.; Pereira, M. F. R. Influence of the Surface Chemistry of Multiwalled Carbon Nanotubes on the Selective Conversion of Cellulose into Sorbitol. *ChemCatChem* **2017**, *9* (5), 888−896.
(31) Yao, N.; Cai, Y.; Li, J.; Nulahong, A.; Okitsu, K.; Xu, F.; Muhammad, I.; Abulizi, A.; Ren, T. Enhanced Low-Temperature Performance of CO2Methanation over Ni-Y Zeolite Molecular Sieve. *J. Environ. Chem. Eng.* **2025**, *13* (5), No. 118415.
(32) Jiang, Z.; Jiang, W.; Yang, B.; Wang, F.; Tu, Z.; He, B.; Zu, Y. An Eco-Friendly Strategy to Upcycle Fluorinated Silica Slag into High-Value ZSM-5 Zeolite and CaF2 for Efficient Fluorine and Silicon Recovery. *Chem. Eng. J.* **2025**, *522*, No. 167252.
(33) Al-Thawabeia, R. A.; Hodali, H. A. Use of Zeolite ZSM-5 for Loading and Release of 5-Fluorouracil. *J. Chem.* **2015**, *2015* (1), No. 403597, DOI: 10.1155/2015/403597.
(34) Hammond, C.; Padovan, D.; Tarantino, G. Porous Metallosilicates for Heterogeneous, Liquid-Phase Catalysis: Perspectives and Pertaining Challenges. *R. Soc. Open Sci.* **2018**, *5* (2), No. 171315.
(35) Wang, C.; Xie, T.; Kots, P. A.; Vance, B. C.; Yu, K.; Kumar, P.; Fu, J.; Liu, S.; Tsilomelekis, G.; Stach, E. A.; Zheng, W.; Vlachos, D. G. Polyethylene Hydrogenolysis at Mild Conditions over Ruthenium on Tungstated Zirconia. *JACS Au* **2021**, *1* (9), 1422−1434.
(36) Dhaniswara, T. K.; Sardi, B.; Juliastuti, S. R.; Mahfud, M. Non-Catalytic and Catalytic Pyrolysis of Polystyrene, Polypropylene, and Polyethylene for Liquid Fuel Production Using a Reactor Integrated with a Fractionation Column. *Cleaner Waste Syst.* **2025**, *11*, No. 100305.
(37) Khan, S.; Lup, A. N. K.; Qureshi, K. M.; Abnisa, F.; Daud, W. M. A. W.; Patah, M. F. A. A Review on Deoxygenation of Triglycerides for Jet Fuel Range Hydrocarbons. *J. Anal. Appl. Pyrolysis* **2019**, *140*, 1−24.
(38) Zhao, Z.; Li, Z.; Zhang, X.; Li, T.; Li, Y.; Chen, X.; Wang, K. Catalytic Hydrogenolysis of Plastic to Liquid Hydrocarbons over a Nickel-Based Catalyst. *Environ. Pollut.* **2022**, *313*, No. 120154.

https://doi.org/10.1021/acssuschemeng.5c12040
ACS Sustainable Chem. Eng. 2026, 14, 4042−4052